

Geometric phases of water waves

F. FEDELE¹

¹ *School of Civil and Environmental Engineering, School of Electrical and Computer Engineering
Georgia Institute of Technology - Atlanta 30332, Georgia, USA*

PACS 92.10.Hm – Ocean waves and oscillations
PACS 02.40.Dr – Euclidean and projective geometries
PACS 03.65.Vf – Phases: geometric; dynamic or topological

Abstract – Recently, Banner et al. (2014) highlighted a new fundamental property of open ocean wave groups, the so-called crest slowdown. For linear narrowband waves, this is related to the geometric phase associated with the parallel transport through the principal fiber bundle of the wave motion with U(1) group symmetry. The theoretical predictions are shown to be in fair agreement with ocean field observations.

Introduction. – Several studies over the past two decades suggest that the initial speed of breaking crests of dominant open ocean wave groups, or breaker speeds, are typically 20% lower than expected from linear wave theory [1]. A recent study in [2] explains the reduced breaker speed by means of the crest slowdown, a new fundamental property of non-breaking ocean waves as they occur naturally, not as uniform wavetrains, but within evolving groups. Before the focusing point, the crest of the largest wave in the group slows down as it advances leaning forward, and it becomes symmetrical as the maximum height is approached. As the wave decays after focus, the crest accelerates as it leans backward. The crest slowdown and the corresponding forward/backward leaning are generic features of each crest of water wave groups. They are associated with the energy convergence in the neighborhood of the focal region, irrespective of whether the wave evolves to break or not [3]. These findings have been validated by means of ocean field observations obtained by the state-of-the-art stereo imaging ([4] and references therein). In particular, the observed probability density function of the crest speed c estimated from all the measured crests peaks at close to $0.8c_0$, with c_0 denoting the phase speed at the spectral peak [2].

In this letter, I will show that the crest slowdown is induced by the natural dispersion of unsteady wave groups. Drawing from quantum mechanics, it can be explained in terms of geometric phases [5–7].

The remainder of the letter is organized as follows. First, I will discuss the crest slowdown of deep-water linear

waves. The geometric interpretation of the wave motion governed by the linear Schrodinger (LS) equation (e.g. [8]) is then presented. This is followed by a comparison with experimental results and conclusions.

Crest slowdown. – If η is the surface displacements, a generic broadbanded linear (small steepness) wave group with no restriction on the spectral bandwidth is given by [9]

$$\eta = \frac{h}{\sigma^2} \int S(\omega) \cos(k(\omega)x - \omega t) d\omega, \quad (1)$$

where $S(\omega)$ is the wave spectrum with variance σ^2 , spectral bandwidth ν , dominant wavenumber k_0 and frequency ω_0 , h is the maximum crest height and $k = \omega^2/g$ in deep water. In particular, the wave group attains its maximal crest height at the focal point ($x = 0, t = 0$) by a constructive superposition of a large number of elementary waves, whose amplitudes depend upon the assumed spectrum $S(\omega)$. The speed c of a crest, where $\partial_x \eta = 0$, is given by [10]

$$c = -\frac{\partial_{xt}\eta}{\partial_{xx}\eta}. \quad (2)$$

From (1), the minimum c_{min} of c is attained at focus and it is given by the weighted average of the linear phase speed $C(\omega) = \omega/k(\omega) = g/\omega$ of Fourier waves as

$$\frac{c_{min}}{c_0} = \frac{\int S(\omega) k^2 C(\omega) d\omega}{\int S(\omega) k^2 d\omega}, \quad (3)$$

arXiv:1406.0051v1 [physics.ao-ph] 31 May 2014

where $c_0 = \omega_0/k_0 = g/\omega_0$ is the phase speed at the spectral peak. For spectra with Gaussian shape and bandwidth $\nu \leq 1/3$, near the crest maximum

$$\frac{c}{c_0} = \frac{c_{min}}{c_0} + qt^2 + O(t^4) \quad (4)$$

where

$$\frac{c_{min}}{c_0} = \frac{1 + 3\nu^2}{1 + 6\nu^2 + 3\nu^4} = 1 - 3\nu^2 + O(\nu^4), \quad (5)$$

and

$$q = \frac{3}{2} + 18\nu^2 + O(\nu^4), \quad (6)$$

Thus, the crest speed tends to diminish as the focal point is reached and the slowdown increases as the spectrum becomes broadbanded, or ν increases. Thus, the slowdown appears with the modulation of the wavetrain induced by the linear dispersion and it is of $O(\nu^2)$ for narrowband spectra. This analysis reveals that wave dispersion and a small but finite spectral bandwidth is essential for the slowdown to arise. Nonlinear effects limit the crest slowdown by reducing wave dispersion (see [3]). Indeed, the linear phase speeds $C(\omega)$ of a Fourier wave in (3) tend to increase with its amplitude $A_f(\omega)$, viz. $C(\omega) \rightarrow C(\omega)(1 + (kA_f)^2)$.

In the following, drawing from differential geometry I will study the behavior of the crest slowdown in linear narrowband wave groups in terms of geometric phases.

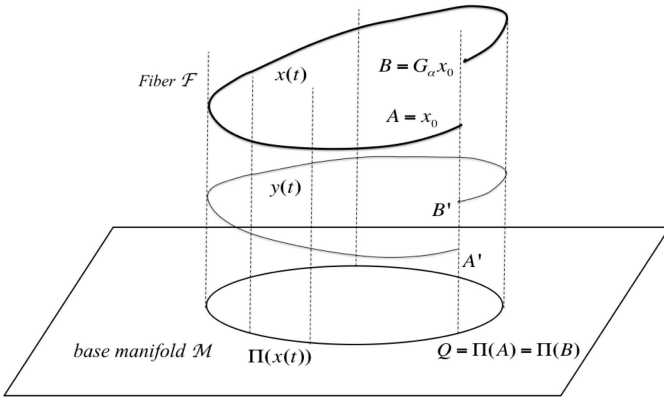


Figure 1: Principal fiber bundle: a relative periodic orbit (RPO) $x(t)$ (AB) reduces to a periodic orbit (PO) in the base manifold \mathcal{M} by properly phase-shifting the trajectory along the fiber \mathcal{F} (or Lie-group space). The shift is composed by a dynamical and geometric phases. The shift induced by the dynamical phase yields the comoving trajectory $y(t)$ ($A'B'$), which is locally transversal to the fibers (parallel transport through the fiber bundle), but it is not a closed trajectory. A further shift by the geometric phase projects $y(t)$ onto the PO on the base manifold \mathcal{M} .

Geometric phases. — They arise due to anholonomy, that is global change without local change. The classical example is the parallel transport of a vector on a sphere.

The change in the vector direction is equal to the solid angle of the closed path spanned by the vector and it can be described by Hannay’s angles [11]. The rotation of Foucault’s pendulum can also be explained by such an anholonomy. Pancharatnan discovered this effect for polarized light [12] and later on Berry rediscovered it for quantum-mechanical systems [5]. It has a geometrical interpretation in terms of principal fiber bundles [6,7,13,14].

In particular, consider a wave motion governed by a dynamical system with continuous Lie-group symmetries. The geometric structure of its state space $\mathcal{P} \in \mathbb{R}^N$ is that of a principal fiber bundle: a base manifold \mathcal{M} of dimension $N - 1$ (quotient space) and one dimensional (1-D) fibers attached to any point p of \mathcal{M} . The fiber \mathcal{F} is the sub-space of the Lie group orbit associated to a point p of \mathcal{M} , viz. points of the fiber \mathcal{F} are Lie-group shifted copies of p . For example, the Euclidean space \mathbb{R}^3 can be seen as a fiber bundle of parallel straight lines. The base manifold is a plane cutting the whole set of parallel lines. This is a trivial fibration since the total space \mathcal{P} is both locally and globally the direct product of the base \mathcal{M} and the fiber \mathcal{F} , that is $\mathbb{R}^3 = \mathbb{R}^2 \times \mathbb{R}$. A famous non trivial fiber bundle is the Hopf fibration of S^3 spheres by great circles S^1 and base space S^2 . The Hopf fibration, like any fiber bundle, is locally a product space, i.e. $S^3 = S^2 \times S^1$, but not globally.

A principal fiber bundle is denoted with the quadruplet $(\mathcal{P}, \mathcal{M}, G_\alpha, \Pi)$ with total space \mathcal{P} over the base manifold \mathcal{M} , and a Lie group G_α , with parameter $\alpha \in \mathbb{R}$, acting on the right on \mathcal{P} , viz. an element of the group of z is $G_\alpha z$. The fiber attached to a point z of \mathcal{M} is the one-dimensional (1-D) Lie group orbit $G_\alpha z$. One can think of the group as being an action, which pushes points in the bundle around the bundle along the fibers (see Fig. 1). To describe this fibration, define the map $\Pi : \mathcal{P} \xrightarrow{G_\alpha} \mathcal{M}$ that projects an element z of the state space \mathcal{P} and all the elements of the group orbit $G_\alpha(z)$ into the same point $\Pi(z)$ of the base manifold \mathcal{M} , viz. $\Pi(z) = \Pi(G_\alpha z)$, with $\alpha \in \mathbb{R}$. In \mathcal{P} , a trajectory $x(t)$ can be observed in a special comoving frame, from which the motion is an horizontal transport through the fiber bundle, that is the comoving trajectory $y(t)$ is locally transversal to the fibers (see Fig. 1). The proper shift along the fibers to bring the motion in the comoving frame is called dynamical phase. This increases with the time spent by the trajectory to wander around \mathcal{P} and system’s answer to: ” how long did your trip take? ”. For example, the translational shift induced by the constant speed of a traveling wave (TW), or relative fixed point, is the dynamical phase. A TW in state space projects onto the base manifold \mathcal{M} reducing to a fixed point, whereas a relative periodic orbit (RPO) reduces to a periodic orbit (PO) (see Fig. 1). In this case, the shift along the fibers necessary to project a RPO onto the based manifold \mathcal{M} includes also a geometric phase, induced by the projected periodic motion [6, 12, 13]. This phase is independent of time and it depends only upon the

geometry of \mathcal{M} , and system's answer to:" where have you been? ". Note that non-periodic orbits in \mathcal{M} induce also a geometric phase [14], that is the wave motion does not have to be periodic to have geometric drift. In summary, the total phase associated with any orbital path on the base manifold is a measure of the motion induced within the fibers of the bundle by the path.

Linear narrowband waves . – Without loosing generality, consider a carrier wave $e^{i(x-t)}$ in deep water. In a reference frame moving at the group velocity $c_g = 1/2$, the wave surface displacements η is given by

$$\eta = B(\xi, t)e^{i(x-t)} + \text{c.c.}, \quad (7)$$

where $\xi = x - t/2$, and the envelope B satisfies the linear Schrodinger (LS) equation (e.g. [8])

$$i\partial_t B = \frac{\delta \mathcal{H}}{\delta \bar{B}} = \partial_{\xi\xi} B. \quad (8)$$

Here, δ denotes variational differentiation,

$$\mathcal{H} = \int |\partial_{\xi} B|^2 d\xi \quad (9)$$

is the Hamiltonian and \bar{B} is the complex conjugate of B . \mathcal{H} is an invariant of the motion, and so are the action and momentum

$$\mathcal{A} = \int |B|^2 d\xi, \quad \mathcal{K} = \text{Im} \int \bar{B} \partial_{\xi} B d\xi. \quad (10)$$

Note that B is slowly varying, viz. its spectral bandwidth ν must be small. The LS equation (8) enjoys the $U(1)$ group symmetry G_{θ} and the translation symmetry G_s . If B is a solution of (8) so are $G_{\theta}(B) = B \exp(i\theta)$ and $G_s(B) = B(\xi + s, T)$, with θ and s any real number. These symmetries reflect the invariance of \mathcal{A} and \mathcal{K} , respectively. G_s is not relevant to the crest slowdown, since it does not induce any dynamical or geometric phase. Hereafter, I will consider only G_{θ} whose group tangent space at B is

$$T(B) = (G_{\theta}^{-1} \partial_{\theta} G)B = iB. \quad (11)$$

Consider now a solution space \mathcal{P} given by the special class of Gaussian envelopes

$$B = a(t) \exp(i\xi^2 \beta(t) - \xi^2 \gamma(t)), \quad (12)$$

and wave surfaces

$$\eta = B \exp(i\xi + i\phi(t)) + \text{c.c.}, \quad (13)$$

where the phase $\phi(t) = -t/2$. From (8), the triplet $z(t) = [a(t), \beta(t), \gamma(t)]$ satisfies the system of ordinary differential equations (ODEs)

$$\frac{dz}{dt} = N(z), \quad (14)$$

with $N(z) = [2ia(\gamma - i\beta), 4(\beta^2 - \gamma^2), 8\gamma\beta]$. Here, $a \in \mathbb{C}$, $(\gamma, \beta) \in \mathbb{R}$, and

$$\mathcal{A} = \sqrt{\frac{\pi}{2}} \frac{|a|^2}{\sqrt{\gamma}}, \quad \mathcal{H} = \sqrt{\frac{\pi}{2}} \frac{|a|^2}{\sqrt{\gamma}} \left(\frac{\beta^2 + \gamma^2}{\gamma} \right), \quad \mathcal{K} = 0 \quad (15)$$

are the three invariants inherited from the LS equation (8), where $|a|$ denotes the absolute value of a . The analytical solution of (14) follows as

$$a = \frac{h}{\sqrt{1 - 2i\nu^2 t}}, \quad \gamma = \frac{1}{2} \frac{\nu^2}{1 + 4\nu^4 t^2}, \quad \beta = \frac{\nu^4 t}{1 + 4\nu^4 t^2}, \quad (16)$$

with h denoting the maximum wave crest height attained at the focusing point ($\xi = 0, t = 0$). The G_{θ} symmetry is also inherited, viz. if z is a solution so is $\tilde{G}_{\theta} z = (a \exp(i\theta), \beta, \gamma)$. The respective group tangent at z is

$$\tilde{T}(z) = (\tilde{G}_{\theta}^{-1} \partial_{\theta} \tilde{G})z = (iz_1, 0, 0) = i(a, 0, 0), \quad (17)$$

where z_1 is the first entry of z . The trajectory $z(t)$ associated with B wanders in the state space $\mathcal{P} \in \mathbb{R}^4 = \mathbb{C} \times \mathbb{R}^2$, which geometrically can be represented as a principal fiber bundle $(\mathcal{P}, \mathcal{M}, G_{\theta}, \Pi)$. The corresponding path or desymmetrized trajectory $Z(t)$ in the base manifold $\mathcal{M} \in \mathbb{R}^3$ is given by the map

$$Z(t) = \Pi(z) = (A(t), \beta(t), \gamma(t)), \quad (18)$$

where $A(t) = |a(t)|$ is the absolute value of a and (γ, β) are the same as in z . From (14), the motion in \mathcal{M} is governed by the ODEs

$$\frac{dZ}{dt} = N_0(Z), \quad (19)$$

where $N_0(Z) = [2A\beta, 4(\beta^2 - \gamma^2), 8\gamma\beta]$. From the invariants (15), the motion occurs on the manifold

$$\beta^2 + \gamma^2 = rA^4, \quad (20)$$

where the constant $r = 2\mathcal{H}/(\pi\mathcal{A}^3)$ (see Fig. 2). The corresponding desymmetrized envelope

$$E(\xi, t) = E(Z) = A(t) \exp(i\xi^2 \beta(t) - \xi^2 \gamma(t)), \quad (21)$$

and wave surface

$$\eta_E(Z) = E(\xi, t) \exp(i\xi) + \text{c.c.} \quad (22)$$

Given the desymmetrized path $Z(t)$ in \mathcal{M} , the original trajectory $z(t)$ can be determined by properly phase-shifting Z along the fibers, viz.

$$z = (a, \beta, \gamma) = \tilde{G}_{\theta} Z = (A \exp(i\theta), \beta, \gamma), \quad (23)$$

where $\theta(t)$ is the phase-shift (see Fig. 1). Thus, from (12) the associated envelope B in space \mathcal{P} depends upon Z as

$$B(Z) = E(Z) \exp(i\theta), \quad (24)$$

and from (13) the wave surface

$$\eta = \eta_E(Z) \exp(i(\theta + \phi)). \quad (25)$$

The phase shift θ depends upon the projected motion in \mathcal{M} induced by both the path Γ generated by the motion $Z(t)$ and the dynamics dictated by (8). To find θ , recall that $E(Z)$ is locally transversal to the fibers. From (11), $\partial_t E$ must be orthogonal to the group tangent space $T(E)$, viz.

$$\overline{T(E)}\partial_t E = i\overline{E}\partial_t E = 0. \quad (26)$$

The governing equation for E follows from (8) as

$$i\partial_t E - \frac{d\theta}{dt}E = \partial_{\xi\xi}E. \quad (27)$$

To impose (26), multiply both members by \overline{E} as

$$i\overline{E}\partial_t E - \frac{d\theta}{dt}|E|^2 = \overline{E}\partial_{\xi\xi}E, \quad (28)$$

and choose

$$\frac{d\theta}{dt} = \frac{d\theta_d}{dt} + \frac{d\theta_g}{dt}, \quad (29)$$

where the dynamical phase θ_d satisfies

$$\frac{d\theta_d}{dt} = -\Omega_d = -\frac{\text{Re}[\overline{E}\partial_{\xi\xi}E]}{|E|^2} \quad (30)$$

and the geometric phase θ_g is given by

$$\frac{d\theta_g}{dt} = -\Omega_g = -\frac{\text{Im}[\overline{E}\partial_t E]}{|E|^2}. \quad (31)$$

Here, Ω_d and Ω_g are corrections of the constant carrier wave frequency as a result of both the LS dynamics and the curvature of the manifold \mathcal{M} (see Eq. 20 and Fig. 2).

Note that the 1-forms in (30) are invariant under the group action, and θ_d can also be determined from the envelope B . In particular,

$$\frac{d\theta_d}{dt} = -\Omega_d = -\frac{\text{Re}[\overline{B}\partial_{\xi\xi}B]}{|B|^2} = \frac{\beta^2 + \gamma^2}{\gamma} = \frac{\mathcal{H}}{\mathcal{A}}. \quad (32)$$

As a result, Ω_d is constant and the dynamical phase increases linearly with the time spent by the trajectory $z(t)$ to wander around \mathcal{P} , viz.

$$\theta_d(t) = \theta_0 + \frac{\mathcal{H}}{\mathcal{A}}t, \quad (33)$$

where θ_0 is an arbitrary constant, which fixes the gauge of freedom (see, for example, [15]).

If I just account for the dynamical θ_d , the comoving trajectory $w(t) = (A\exp(-i\theta_d), \beta, \gamma)$ associated with the envelope $B_c = G_{-\theta_d}(B) = B\exp(-i\theta_d)$ moves through the fiber bundle locally transversal to the fibers. This motion is referred to as the horizontal transport through the fiber bundle and it satisfies $\overline{T(B_c)}\partial_t B_c = 0$ (see Eq. 26).

The comoving envelope B_c still experiences a phase shift, the geometric θ_g given by (31). Indeed, the desymmetrized envelope E associated with the trajectory $Z(t)$ on the base manifold \mathcal{M} is obtained by further shifting B_c along the fibers by θ_g , viz. $E = G_{-\theta_g}(B_c) = G_{-\theta_d-\theta_g}(B)$. Indeed, from (31) and (19)

$$\frac{d\theta_g}{dt} = -\frac{\text{Im}[\overline{E}\partial_t E]}{|E|^2} = -\frac{\text{Im}[\overline{E}\partial_Z E \frac{dZ}{dt}]}{|E|^2} = -\frac{1}{4\gamma} \frac{d\beta}{dt} \quad (34)$$

and the geometric phase θ_g follows from the contour integral

$$\theta_g = -\int_{\Gamma} \frac{\text{Im}[\overline{E}\partial_Z E dZ]}{|E|^2} = -\int_{\Gamma} \frac{1}{4\gamma} d\beta, \quad (35)$$

where Γ is the path in \mathcal{M} generated by the motion $Z(t)$ (see Fig. 2). Clearly, the geometric phase is independent of time and it depends only upon the path on the base manifold [5, 6, 13].

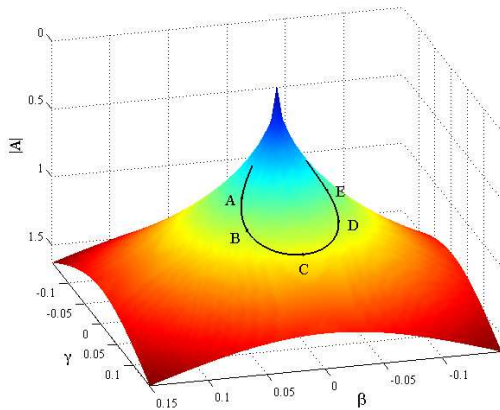
The crest speed c/c_0 varies in time because of the dependence upon the geometric phase θ_g as

$$\frac{c}{c_0} \approx 1 - \frac{d(\theta_d + \theta_g)}{dt} = 1 + \Omega_d + \Omega_g = 1 - \frac{\mathcal{H}}{\mathcal{A}} + \frac{1}{4\gamma} \frac{d\beta}{dt}. \quad (36)$$

Since the dynamical component Ω_d is constant in time, the slowdown is purely induced by the geometric component Ω_g associated with the dynamics on the base manifold \mathcal{M} . This corresponds to a reshaping of the wave surface, which first leans backward and then forward as described below.

The projected wave motion $Z = \Pi(z)$ onto \mathcal{M} is shown in Fig. 2 at different instants of time or stages of the wave group evolution. The associated desymmetrized envelope $|E|$ and wave surface η_E are shown in the right-panel of Fig. 3. The corresponding $|B|$ and η in \mathcal{P} are reported in the right panel of the same figure. The latter shows that before the focusing point (stage A), the largest wave in the group advances leaning forward (stage B), and it becomes symmetrical as the maximum height is approached (stage C). As the wave group grows, the crest slows down and then it accelerates as it leans backward (stage D) as the wave decays after focus (stage E). To quantify the crest profile asymmetries, I define the leaning coefficient $\lambda = d_R/d_L$, where d_R (d_L) is the distance between the crest location and the adjacent zero down-crossing (zero up-crossing). Thus, before (after) focus, $\lambda < 1$ ($\lambda > 1$) because the crest lean forward (backward) while decelerates (accelerates). At focus, $\lambda = 1$ and the crest is symmetric with null acceleration. Note that λ is the same for both η and η_E .

In contrast, the dynamics on the base manifold \mathcal{M} does not present any drift since the desymmetrized wave envelope $|E|$ does not travel along ξ (see left panel of Fig. 3). However, the wave surface η_E features crest asymmetries due to forward/backward leaning associated with


 Figure 2: Projected path Z on the base manifold \mathcal{M} .

the dynamics on \mathcal{M} (see Fig. 2). This induces the crest slowdown as clearly seen in Fig. 4, which shows the crest speed c/c_0 and the wave steepness $\varepsilon = 2\pi/Lh$ as function of the leaning coefficient λ , with L and h denoting the local crest amplitude and wavelength respectively. As a result, theory predicts that the maximum crest slowdown occurs when the crest is the largest in the group with maximum steepness and it has a symmetric profile, viz. $\lambda = 1$. In the following, the theoretical predictions will be compared against ocean field measurements.

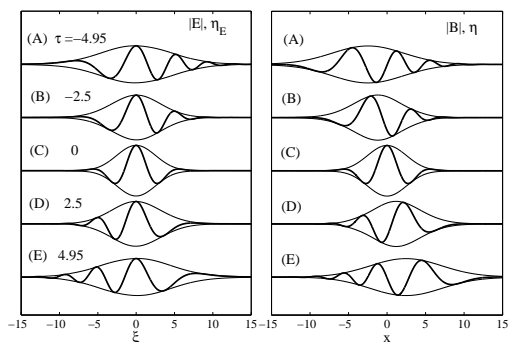


Figure 3: Wave group evolution ($\nu = 0.2$): (left) envelope $|E|$ and wave surface η_E associated to the path $Z(t)$ on the base manifold \mathcal{M} at the different time instants or stages indicated in Fig. 2; (right) same for the envelope $|B|$ and wave surface η associated to the path $z(t)$ on the original space \mathcal{P} . The maximum wave crest is attained at $t = 0$ (stage C).

Ocean field observations. – The Wave Acquisition Stereo System (WASS) was deployed at the oceanographic tower Acqua Alta located in the Northern Adriatic Sea, 10 miles off the coastline of Venice, on 16 meters deep waters [16]. Video measurements were acquired in three experiments carried out during the period 2009-2010 to investigate both space-time and spectral properties of oceanic waves ([4] and references therein). To maximize the common field of view of the two cameras, WASS cameras were 2.5 m apart, 12.5 m above sea level at 70° depression an-

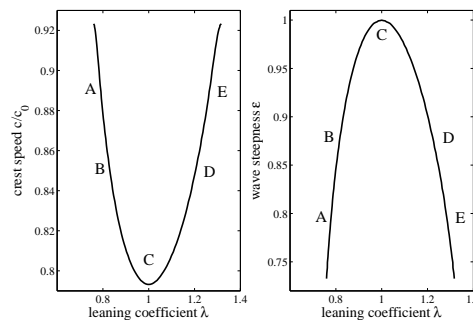


Figure 4: (Left) crest speed c/c_0 and associated (right) wave steepness ε as function of the leaning coefficient λ at the different stages of the wave group evolution (see Figs. 2,3).

gle, providing a trapezoidal area with sides of length 30 m and 100 m, respectively, and a width of 100 m.

In this work, I elaborated the stereo data acquired during Experiment 2, viz. 21000 snapshots at 10 Hz. The mean windspeed was 9.6 m/s with a 110 km fetch, and the unimodal wave spectrum had a significant wave height $H_s = 1.09$ m and dominant period $T_p = 4.59$ s. Most observed crests were very steep, with sporadic spilling breaking. The data were filtered above 1.5 Hz to remove short riding waves. The speeds c of crests observed within the imaged area were estimated by tracking the space crest along the dominant wave direction. Subpixeling reduced quantization errors in estimating the local crest position and the leaning coefficient λ . The local reference speed c_0 was calculated from the peak frequency of the short-term Fourier spectrum of a time series of duration D centered at the crest event ($D = 120$ s as an optimal record length) and Doppler corrected for the in-line 0.20 m/s mean current. Fig. 5 reports the observed conditional mean value as function of λ and stability bands of the wave steepness ε (left panel) and speed c/c_0 (right panel) of dominant local wave crests with elevations $h > 0.3h_{max}$, with h_{max} denoting the maximum crest height. In average, the maximum wave steepness is attained for symmetric crest profiles ($\lambda \approx 1$) and the crest speed is the lowest at $\lambda \approx 0.8$ with minimum $c/c_0 \approx 0.83$. These results are in fair agreement with the above described theory, although the maximum slowdown is observed for crests that are slightly leaning forward, whereas theory predicts a symmetric profile, viz. $\lambda = 1$. One may argue that this is an ideal condition since the probability to observe a symmetric crest, which is also the maximum of a wave group (perfect focusing) is practically null (see, for example, [9]).

Conclusions. – The crest slowdown is basically a linear phenomenon induced by the dispersive nature of unsteady wave groups. Drawing from quantum mechanics, for linear narrowband waves it has a simple geometric in-

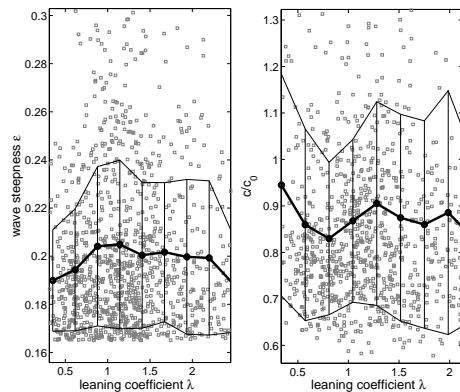


Figure 5: WASS observations: (left) average local steepness ε and (right) crest speed c/c_0 as function of the leaning coefficient λ .

terpretation in terms of the geometric phase associated with the wave motion with $U(1)$ group symmetry. The role of nonlinear effects on the crest slowdown is still an open research. In this regard, initial studies within the framework of the Zakharov equation [3] indicate that nonlinearities limit the slowdown effect by dispersion reduction, that is phase speeds of high-frequency harmonic waves increase relative to their linear counterparts. Further studies are desirable to investigate how the associated dynamical and geometric phases are affected by nonlinearities.

Acknowledgments. – WASS experiments at Acqua Alta were supported by Chevron (CASE-EJIP Joint Industry Project No. 4545093). FF thanks Prof. Michael Banner for useful discussions on ocean waves and Dr. Alvise Benetazzo for the support with the analysis of WASS data.

References

- [1] RAPP R. J. and MELVILLE W. K., *Philosophical Transactions of the Royal Society of London. Series A, Mathematical and Physical Sciences*, **331** (1990) 735.
- [2] BANNER, M. L., BARTHELEMY X., FEDELE F., ALLIS M., BENETAZZO A., DIAS F. and PEIRSON, W. L., *Phys. Rev. Lett.*, **112** (2014) 114502.
- [3] FEDELE F., *Journal of Fluid Mechanics*, **748** (2014) 692.
- [4] FEDELE F., BENETAZZO A., GALLEGRO G., SHIH P.-C., YEZZI A., BARBARIOL F. and ARDUIN F., *Ocean Modelling*, **70** (2013) 103 .
- [5] BERRY M. V., *Proceedings of the Royal Society of London. A. Mathematical and Physical Sciences*, **392** (1984) 45.
- [6] SIMON B., *Phys. Rev. Lett.*, **51** (1983) 2167.
- [7] SAMUEL J. and BHANDARI R., *Phys. Rev. Lett.*, **60** (1988) 2339.
- [8] MEI C. C., *The applied dynamics of water waves* (World Scientific) 1989.
- [9] FEDELE F. and TAYFUN M., *Journal of Fluid Mechanics*, **620** (2009) 221.
- [10] LONGUET-HIGGINS M. S., *Philosophical Transactions of the Royal Society of London. Series A, Mathematical and Physical Sciences*, **249** (1957) 321.
- [11] HANNAY J. H., *Journal of Physics A: Mathematical and General*, **18** (1985) 221.
- [12] PANCHARATNAM S., *Proceedings of the Indian Academy of Sciences - Section A*, **44** (1956) 247.
- [13] AHARONOV Y. and ANANDAN J., *Phys. Rev. Lett.*, **58** (1987) 1593.
- [14] ANANDAN J., *Nature*, **360** (1992) 307.
- [15] SHAPER A. and WILCZEK F., *Journal of Fluid Mechanics*, **198** (1989) 557.
- [16] BENETAZZO A., FEDELE F., GALLEGRO G., SHIH P.-C. and YEZZI A., *Coastal Engineering*, **64** (2012) 127 .